Thermal properties of high-k $Hf_{1-x}Si_xO_2$*

Si Feng-Juan(司凤娟)[a], Lu Wen-Jiang(路文江)[a], and Tang Fu-Ling(汤富领)[a)b)†]

[a] *State Key Laboratory of Gansu Advanced Non-ferrous Metal Materials, Department of Materials Science and Engineering, Lanzhou University of Technology, Lanzhou 730050, China*

[b] *Key Laboratory of Non-ferrous Metal Alloys and Processing of Ministry of Education, Lanzhou University of Technology, Lanzhou 730050, China*

(Received 9 November 2011; revised manuscript received 19 January 2012)

Classical atomistic simulations based on the lattice dynamics theory and the Born core-shell model are performed to systematically study the crystal structure and thermal properties of high-k $Hf_{1-x}Si_xO_2$. The coefficients of thermal expansion, specific heat, Grüneisen parameters, phonon densities of states and Debye temperatures are calculated at different temperatures and for different Si-doping concentrations. With the increase of the Si-doping concentration, the lattice constant decreases. At the same time, both the coefficient of thermal expansion and the specific heat at a constant volume of $Hf_{1-x}Si_xO_2$ also decreases. The Grüneisen parameter is about 0.95 at temperatures less than 100 K. Compared with Si-doped HfO_2, pure HfO_2 has a higher Debye temperature when the temperature is less than 25 K, while it has lower Debye temperature when the temperature is higher than 50 K. Some simulation results fit well with the experimental data. We expect that our results will be helpful for understanding the local lattice structure and thermal properties of $Hf_{1-x}Si_xO_2$.

Keywords: thermal properties, lattice structure, high-k material

PACS: 65.40.Ba, 63.10.+a, 63.20.–e **DOI:** 10.1088/1674-1056/21/7/076501

1. Introduction

More integrated complementary metal-oxide-semiconductor transistor (CMOS) devices need high dielectric constant (high-k) materials which can replace traditional dielectric SiO_2 to reduce the leakage current and impurity diffusion. High-k materials also inhibit the tunneling effect.[1,2] Among the alternative high-k materials, HfO_2 is a promising material with a relatively high dielectric constant, wide band gap, high thermal stability, high melting point, excellent compression performance and low thermal expansion coefficient.[3–5] In a CMOS device, a Si atom in the base material can diffuse into the high-k layer and its doping into HfO_2 can improve its technological properties. In addition, it can be used as not only a high-k material but also a thermal barrier coating. Dielectric materials should withstand very high temperatures for a long time, so as to acquire the thermal properties of the Si-doped HfO_2 at different temperatures, which is particularly important.[6,7]

Under atmospheric pressure, HfO_2 has three crystal types: cubic HfO_2 (c-HfO_2, space group: $Fm3m$) at high-temperatures, tetragonal HfO_2 (t-HfO_2, $P4_2/nmc$) at moderate temperatures, and monoclinic HfO_2 (m-HfO_2, $P2_1/c$) at and below room temperature.[8–10] Recently, more theoretical and experimental attention was paid to defects/surfaces in/on the HfO_2[11,12] and HfO_2-Si interface,[13–15] especially to its thermal properties. Medvedeva *et al.*[16] calculated the band gap, binding energy, lattice vibrations, and dielectric properties. Carav and Casali[17] systematically studied various HfO_2 crystalline structures for their relative stabilities and relationship with pressure. They predicted the phase transitions and some of their results were consistent with the experimental results. Xu *et al.*[18] have also used the first-principles potential plane wave method to calculate the electronic structure and optical properties in c-HfO_2 and t-HfO_2. Zheng *et al.*[19] have investigated m-HfO_2 for point defects of oxygen. Though comprehensive theoretical studies have largely concentrated on the stability of different phases and the electric and dielectric properties as seen above, other basic

*Project supported by the National Natural Science Foundation of China (Grant Nos. 10964003 and 11164014), the Natural Science Foundation of Gansu Province, China (Grant No. 096RJZA102), the Specialized Research Fund for the Doctoral Program of Higher Education, China (Grant No. 20096201120002), and the China Postdoctoral Science Foundation (Grant Nos. 20100470886 and 201104324).

†Corresponding author. E-mail: tfl03@mails.tsinghua.edu.cn

physical properties, such as the mechanical and thermal properties of high-k $Hf_{1-x}Si_xO_2$ are still rarely studied. Moreover, the overall performance of high-k HfO_2 under a high temperature and pressure are particularly important for their technical applications. In a high temperature CMOS technical process, this material may bring on cracking, distortion, and loss introduced by thermal expansion mismatch.

2. Simulation methods

Our simulation is based on the widely used successful core-shell model generalization of the Born model of a solid. We have used the atomistic simulation technique to study the local lattice structures, Jahn–Teller distortions and thermal properties of $LaMnO_3/SrMnO_3$[20,21] and their superlattices with different Sr concentrations.[22] Using these methods, we study the thermal properties of $Hf_{1-x}Si_xO_2$, including the lattice constants, specific heat, elastic constants, coefficients of thermal expansion, Grüneisen parameters, and Debye temperatures at different temperatures and for different Si-doping concentrations. Within Born's core-shell model, the lattice energy E at 0 K can be expressed as

$$E = \frac{1}{2}\sum_{i,j}\left[\frac{q_i q_j}{r_{ij}} + V(r_{ij})\right], \tag{1}$$

where q_i is the charge on ion i, q_j is the charge on ion j, and r_{ij} is the distance between these two ions. In Eq. (1), the first item is the Columbic energy introduced by long range interactions of effective charges, and the second item is the short range interactions. The short-range interactions are represented by the Buckingham potential, which is a function of the distance between two ions r_{ij}, and is given as

$$V(r_{ij}) = A\exp(-r_{ij}/\rho) - Cr_{ij}^{-6}, \tag{2}$$

where A, ρ, and C are the fitting parameters. In order to describe the polarization of an individual ion and its dependence on the local atomic environment, the core-shell model is used. The interaction between the core and shell of any ion is treated as a harmonic with a spring constant k and is represented by

$$E_{\rm v}(d_i) = \frac{1}{2}kd_i^2, \tag{3}$$

where d_i is the relative displacement of the core and shell of ion i. The polarization of a massless shell with a Y charge and a core with an X charge ($X+Y$ is the charge of the ion) can be calculated as

$$\alpha = \frac{Y^2}{k}, \tag{4}$$

where Y is the charge of the shell and is related to the dielectric constant, and k is the force constant between the core and the shell and is related to the phonon frequency. Both parameters Y and k are fitting parameters.

This method, programmed in the General Utility Lattice Program (GULP),[23] has been used to simulate many kinds of compounds.[23–26] A brief illustration of this technique can be found in Ref. [23] and details are available in Refs. [20]–[22]. It should be stressed that the reliability of our simulation strongly depends on the validity of the potential model used, and the latter is assessed primarily by its ability to reproduce experimental crystal properties. The potential parameters used for cubic-HfO_2 and alpha-quartz SiO_2 are fitted and given in Table 1, and the charge and elastic constants of O^{2-} are $-2.869e$ and 74.92 eV·Å^2, which can reproduce the experimental crystal structure of HfO_2 with small differences in the lattice parameter between the calculated and experimental data (Table 2).[26–28]

Table 1. Potential parameters used for $Hf_{1-x}Si_xO_2$.

	A/eV	ρ/Å	C/eV·Å^6
Hf^{4+}–O^{2-}	1454.6	0.3500	0.000
Si^{4+}–O^{2-}	1283.03767	0.3205	10.660
O^{2-}–O^{2-}	22764.3	0.1490	27.879

Table 2. Comparison between the calculated and experimental lattice constants for SiO_2 and HfO_2.

		Exp.[9,26]	Cal.[9,26]	This work	Error/%
SiO_2	$a=b$/Å	4.916	5.02	4.915	−0.02
	c/Å	5.405	5.54	5.407	0.04
	$L_{\rm Si-O}$/Å[a)]	1.605	1.63	1.640	2.20
	∠O–Si–O	109.4°	–	110.0°	0.55
HfO_2	a/Å	5.08	5.07	5.10	0.39

[a)] $L_{\rm Si-O}$ is the bond length of Si–O.

Our simulation results are similar to the calculated data in Refs. [9] and [26]. The difference in the lattice parameter and bond length of SiO_2 between the calculated and experimental data is less than 0.02 Å.[26] We checked this potential at high temperatures. The potential for HfO_2 and SiO_2 (the potential for SiO_2 is newly fitted based on the same

O–O potential for HfO_2) are checked and they are stable until 1800 K by lattice dynamics. After Si-doping into HfO_2, the simulations are less stable for different doping densities, but they are still stable when the temperature is less than 1500 K, and we used them up to 1500 K.

In this work, the initial structure for studying the Si-doped HfO_2 with a cubic structure has the crystallographic unit cell of HfO_2, which has four Hf^{4+} ions and eight O^{2-}ions. To meet the requirements for the Si-doping ion number proportion and to make the calculations the most efficient, the unit cell of HfO_2 is extended several times along both the *a*-, *b*-, and *c*-axis direction. For simulating the structure of $Hf_{1-x}Si_xO_2$, Hf^{4+} ions are substituted by Si^{4+} ions with different values of doping concentration x.

3. Results and discussion

3.1. Lattice constants

All lattice constants in the two mother materials are fitted and optimized by the GULP program[23] under the free energy minimization principle at 0 K. Using the previous model of the interaction between ions and the lattice dynamics method, we simulate and calculate the lattice structures of $Hf_{1-x}Si_xO_2$ in a temperature range of 0–1500 K and a pressure range of 0–25 GPa in Fig. 1. The lattice constants vary with temperature and pressure as shown in Figs. 1(a) and 1(b) respectively. These curves describe the relationship among the lattice constants, Si-doping concentrations, temperature, and pressure.

From Fig. 1(a), it is found that the lattice constants $a = b = c$ reduce as the Si-doping concentration increases. This is because the ionic radius of Si^{4+} (0.42 Å) is smaller than that of Hf^{4+} (0.72 Å).[29] However, as the temperature gradually increases, the lattice constant increases, that is, thermal expansion in this crystal occurs. As the temperature increases from 0 K to 1500 K, the lattice constant increases less in $Hf_{1-x}Si_xO_2$ with Si-doping concentration than with smaller Si-doping concentrations. This can be confirmed by the coefficients of thermal expansion as below. As can be seen in Fig. 1(b), the lattice parameter a of $Hf_{1-x}Si_xO_2$ decreases as the pressure increases from 0 GPa to 25 GPa. The lattice volume reduction in $Hf_{1-x}Si_xO_2$ with a larger x is more than that with a smaller x, indicating that the former is "softer" than the latter, which is introduced by different lattice energies of HfO_2 and SiO_2, and can affect their Debye temperatures.

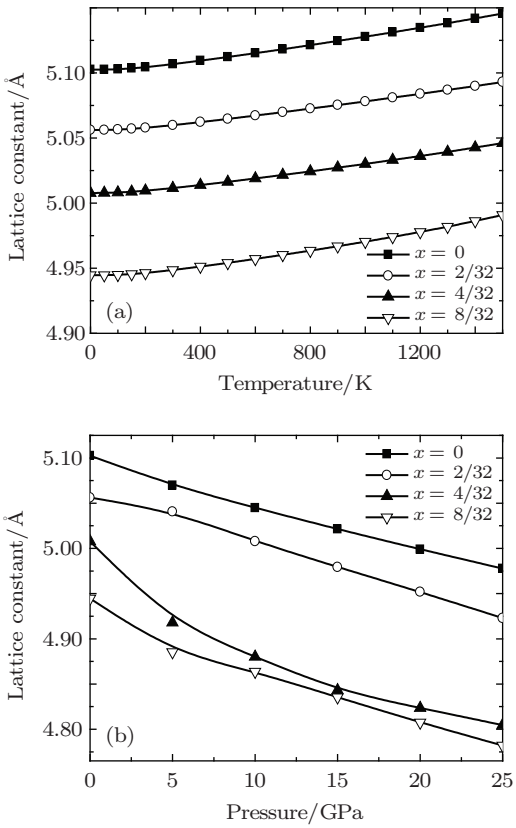

Fig. 1. Lattice constants of $Hf_{1-x}Si_xO_2$ each as a function of temperature (a) and pressure (b).

3.2. Bond length and bond angle

To obtain bond lengths and bond angles in $Hf_{1-x}Si_xO_2$, the orthogonal cubic HfO_2 lattice is used as the original structure. It is expanded into a supercell containing 32 Hf atoms (and 64 O atoms) for Si-doping. The lattice structure is simulated at 0 K with the free energy minimization principle of optimization. Using the previous atomic interactions (Table 1) between Hf^{4+}–O^{2-}, Si^{4+}–O^{2-}, and O^{2-}–O^{2-} ions and the free energy minimization technique, we simulate the local lattice structure of Si-doped HfO_2, i.e., the distribution of the Si–O/Hf–O bond lengths and the O–Si–O/O–Hf–O bond angles for different Si-doping concentrations (Fig. 2).

From Fig. 2(a), it is found that as the Si doping concentration increases from 0 to 1, the number of Si–O bonds increases, while the bond length slightly decreases, although the change is not obvious. The pure SiO_2 bond length distribution concentrates at about 1.8 Å and 3.5 Å. When the doping concentration decreases, the distribution of the bond length extends. Our calculated shortest Si–O bond length corresponds to experimental value (marked with a rectangle in Fig. 2(a)[26,27]).

Due to the fact that the O^{2-} binding energy to Hf^{4+} is different from that to Si^{4+} (Table 1), the incorporation of Si into HfO_2 affects the surrounding Hf–O bond lengths. In Fig. 2(b), the number of Hf–O bonds increases as the doping density decreases from 1 to 0, which is contrary to the case of the Si–O bond shown in Fig. 2(a). At the same time, the bond length becomes larger and the bond length distribution is also extended.

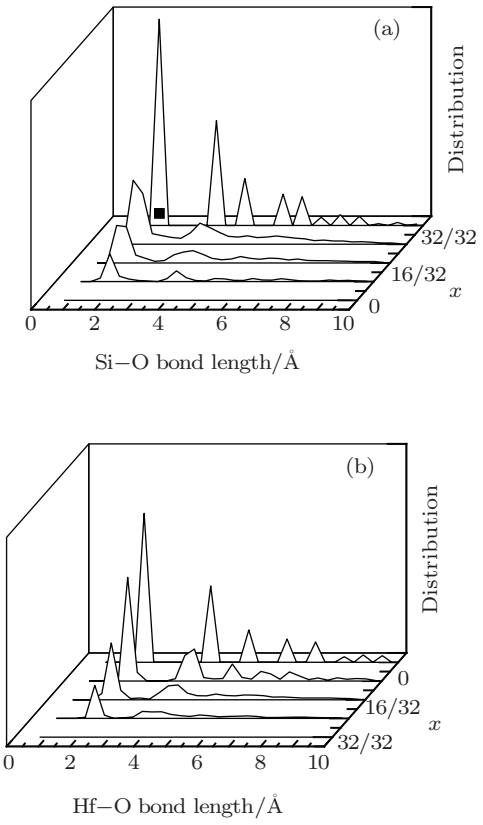

Fig. 2. Bond lengths of (a) Si–O and (b) Hf–O of $Hf_{1-x}Si_xO_2$ (x = 0–1). Symbol ■ indicates Si–O bond length at 2 GPa obtained from the experiment.[26]

We also calculated the bond angles in Si-doped HfO_2. From Fig. 3(a), it is found that as the Si doping concentration x increases, the number of O–Si–O bond angles increases. When $x = 1$, the O–Si–O bond angle distribution in pure SiO_2 concentrates at about 75° and 115°. The O–Hf–O bond angle distribution is similar to that of the O–Si–O angle. If the Si doping density is not 0 or 1, the distribution of the bond lengths and that of the bond angles are extended, indicating that the local lattice structure is not ideally ordered. Our O–Si–O angle around 115° corresponds to the experimental value (marked with the rectangle in Fig. 3(a)[26,27]).

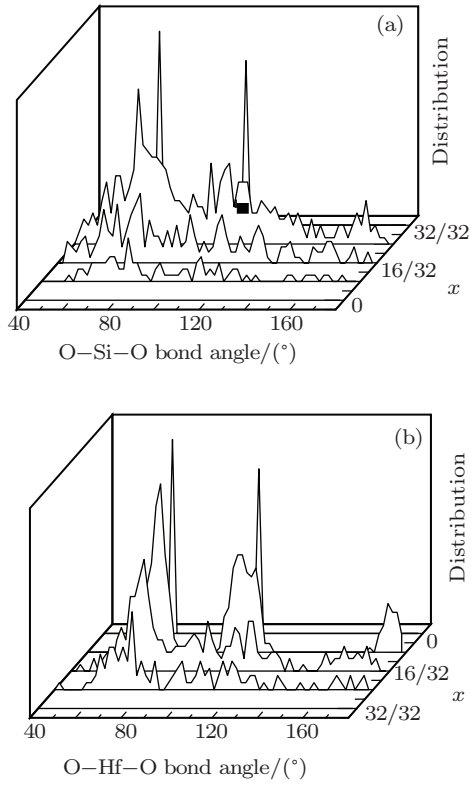

Fig. 3. Bond angle distributions of (a) O–Si and (b) Hf–O of $Hf_{1-x}Si_xO_2$ (x = 0–1), where the symbol "■" denotes the O–Si–O bond angle at 2 GPa obtained from the experiment.[26]

3.3. Elastic modulus

Because elastic modulus is related to the thermal properties (the coefficient of thermal expansion and the Debye temperature), the bulk modulus (K_T) and shear modulus (G) of $Hf_{1-x}Si_xO_2$ are calculated using the unit cell grown twice along the a-, b-, and c-axis (2×2×2), respectively. The variation of the elastic modulus with rising pressure are shown in Fig. 4.

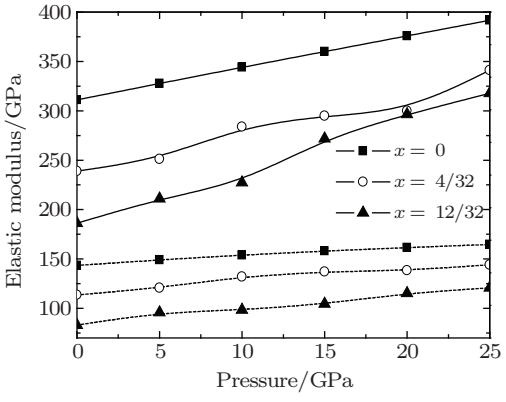

Fig. 4. Elastic moduli of $Hf_{1-x}Si_xO_2$ each as a function of pressure for different Si-doping concentrations, where the solid line (—) and the dotted line (···) denote the bulk modulus (K_T) and the shear modulus (G), respectively.

From Fig. 4, it is found that the bulk modulus and the shear modulus decrease as the Si-doping concentration increases. As the pressure increases, both the bulk modulus and shear modulus increase, and the change of the former is larger than that of the latter. We also find that elastic modulus reduces as the temperature increases (not shown), as the material has a slightly small resistance to the elastic deformation at higher temperatures.[30]

3.4. Specific heat

We calculate the values of specific heat at a constant volume (C_V) at different temperatures when the doping concentrations of $Hf_{1-x}Si_xO_2$ are $x = 0$, 2/32, 4/32 and 8/32 (0–1500 K), which are shown in Fig. 5.

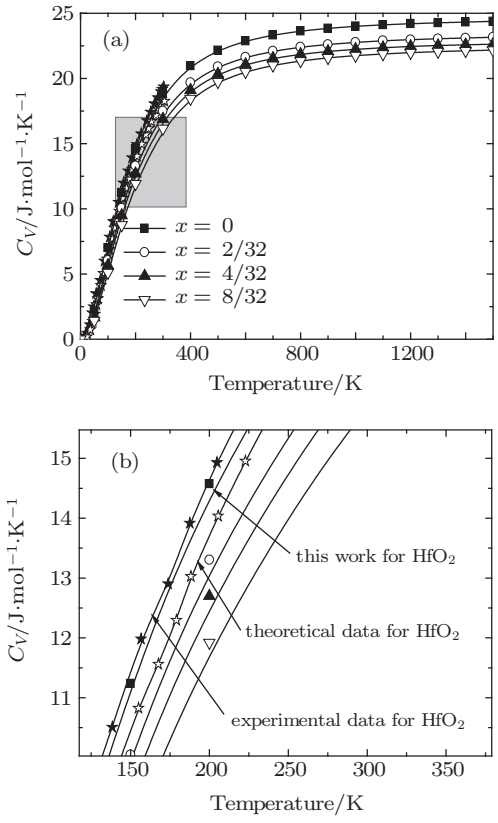

Fig. 5. (a) Plots of specific heat at a constant volume (C_V) of $Hf_{1-x}Si_xO_2$ versus temperature (0–1500 K) at several different Si-doping concentrations (x = 0–8/32), and (b) their enlargements of the shaded part in panel (a).

From Fig. 5, it is found that the values of specific heat (C_V) for $Hf_{1-x}Si_xO_2$ decrease as the Si-doping concentration increases. As the temperature T rises, C_V increases for each doping concentration. The value of C_V rapidly reduces to zero as T approaches 0 K, owing to $C_V \propto T^3$. As the temperature increases to 400 K, the specific heat rapidly increases. When the temperature is greater than 400 K, the values of C_V are all close to the Dulong–Petit limit: 24.94 J·mol^{-1}·K^{-1}. Differences among the values of C_V for different Si-doping concentrations become larger as the temperature increases from 0 K to 1500 K. In Fig. 5, some additional calculated and experimental data[31,32] of the specific heat at constant pressure (C_P) of HfO_2 at temperatures of 0–650 K are also shown. These curves of C_P of HfO_2 match our results.

3.5. Coefficient of thermal expansion

According to Grüneisen law, the formula of the volumetric coefficient of thermal expansion can be drawn (coefficient of thermal expansion, CTE) as[33–36]

$$\alpha_V = \frac{\gamma_V \rho' C_V}{K_T}. \tag{5}$$

In formula (5), ρ' is the density of a solid, C_V is the specific heat of a solid, γ_V is the Grüneisen parameter, taking $\gamma_V = 0.95$ for $Hf_{1-x}Si_xO_2$, and K_T is the bulk modulus. The parameters ρ', C_V, K_T can be directly calculated using the lattice dynamics theory by GULP. We calculate CTE with the crystal structure of an eight-unit cell for a Si-doping concentration of $x = 0$, 2/32, 4/32, 6/32, and 8/32 (Fig. 6(a)).

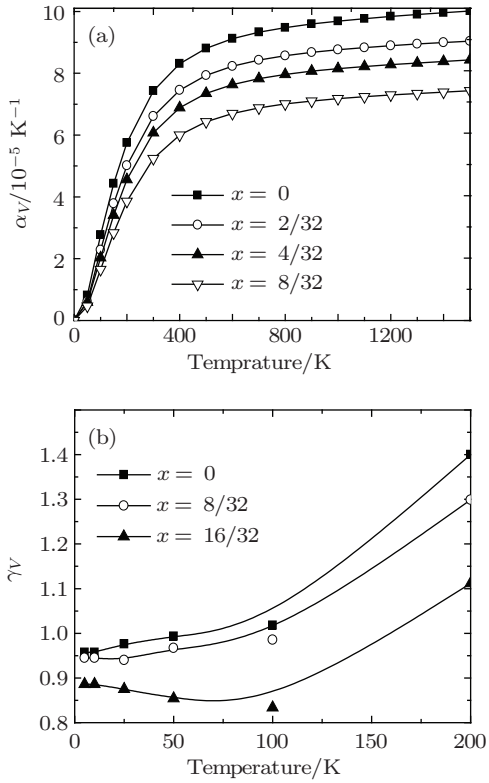

Fig. 6. (a) Volumetric coefficients of thermal expansion (CTE) and (b) Grüneisen parameters of $Hf_{1-x}Si_xO_2$ each as a function of temperature.

From Fig. 6(a), one can find that the volumetric CTE of $Hf_{1-x}Si_xO_2$ will reduce when the Si-doping concentration increases. As the temperature increases, the difference among the volumetric CTEs for different Si-doping concentrations increase. As the Si-doping concentration increases, the density (ρ), specific heat (C_V), and bulk modulus (K_T) all reduce with different degrees, and the volumetric CTE of $Hf_{1-x}Si_xO_2$ reduces. When the temperature is larger than 0 K and smaller than 400 K, α_V increases rapidly; while it increases slowly when the temperature is higher than 400 K. This is because the volumetric thermal expansion of a solid relates to the average distance between adjacent atoms. The potential energy (short-range interaction in Eq. (2)) between two adjacent atoms in the crystal is a function of the distance between different atoms, and the curve of potential energy is non-symmetrical. At a certain temperature, the distance between two atoms changes around the equilibrium distance. Because of the non-symmetry of the curve of potential energy, the average distance r between two atoms is greater than the equilibrium distance r_0. If the temperature rises, i.e., the vibrational energy becomes larger, the average distance will be even longer. As the vibration energy increases with the rise in temperature and the average distance between two atoms increases, then the entire solid will expand and the lattice volume will become larger accordingly.

In order to check the value of the Grüneisen parameter γ_V in formula (5), we use Grüneisen state equation

$$P = -\frac{\mathrm{d}U}{\mathrm{d}V} + \gamma_V \frac{E_\mathrm{v}}{V}, \tag{6}$$

where P is the pressure, U the lattice energy from atomic position, E_v the thermal vibration energy, and V the lattice volume. We take $P = \pm 0.01$ GPa to obtain ΔU and ΔV at lower temperatures, so $\gamma_V = V(P + \frac{\mathrm{d}U}{\mathrm{d}V})/E_\mathrm{v}$ ($P = 0$ GPa, V and E_v takes their average values when P is ± 0.01 GPa at a certain temperature). The results are shown in Fig. 6(b). It is found that γ_V decreases as the Si-doping concentration increases, and has a larger value at higher temperatures. Under a temperature less than 100 K, $\gamma_V \approx 0.95$, and we take this value to calculate the thermal expansion coefficients in $Hf_{1-x}Si_xO_2$ (see Fig. 6).

3.6. Phonon density of states and Debye temperature

In Fig. 5, one can see that the specific heat tends to zero as the temperature reduces to zero. To investigate the relationship among the lattice vibration, specific heat, and Debye temperature, we first calculate total and partial phonon densities of states (DOSs) for different Si-doping concentrations, and show the results in Fig. 7.

From Fig. 7(a), one can find that the phonon spectra of $Hf_{1-x}Si_xO_2$ range from 0 to 800 cm^{-1} wave number. Si-doping moves the phonon spectra towards the left. Hf atoms show a larger energy contribution in the low frequency region, and almost no contribution in the high frequency region (> 400 cm^{-1}); Si atoms, different from Hf atoms, show an energy contribution within the entire frequency region for various Si-doping concentrations. O atoms show larger energy contributions in the higher spectrum range for all Si-doping concentrations (Figs. 7(b)–7(d)).

Within the Debye model, we use the lattice dynamics to calculate the specific heat at a constant volume, and then we can determine Debye temperatures at different temperatures from the following formula:

$$\begin{aligned} C_V &= \left(\frac{\partial \bar{E}}{\partial T}\right)_V \\ &= 9Nk_\mathrm{B}\left(\frac{T}{T_\mathrm{D}}\right)^3 \int_0^{\frac{T_\mathrm{D}}{T}} \frac{y^4\,\mathrm{e}^y}{(\mathrm{e}^y-1)^2}\,\mathrm{d}y. \end{aligned} \tag{7}$$

In formula (7), $y = T_\mathrm{D}/T$, N is the total number of atoms, k_B the Boltzmann constant, T the temperature, and T_D the Debye temperature. We calculate the values of specific heat at a constant volume, for a Si-doping concentration of $x = 0$, 4/32, 12/32, and 16/32. Using formula (7) which describes the relationship between temperature and specific heat, we calculate the values of Debye temperature (T_D) when the temperatures are in a range of 0–300 K, and show the results in Fig. 8.

From Fig. 8, one can find that the values of T_D of $Hf_{1-x}Si_xO_2$ increase as the Si-doping concentration increases at temperatures higher than 50 K, while they decrease with temperature T increasing in a temperature range of 0–25 K. In particular, pure HfO_2 has the lowest T_D when $T > 50$ K, while it has the highest T_D when $T < 25$ K. At 300 K, the values of T_D of $Hf_{1-x}Si_xO_2$ range from 700 K to 800 K. The minimal T_D is about 450 K when the temperature is higher than 25 K but less than 50 K.

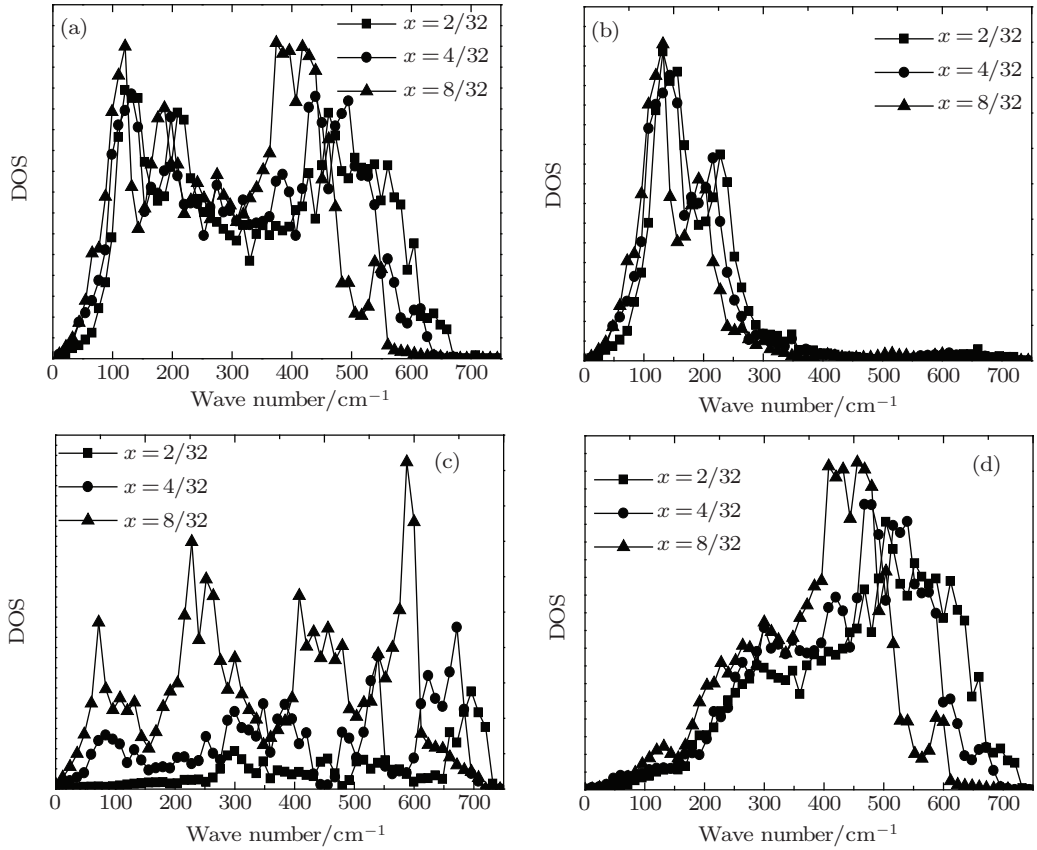

Fig. 7. Total and partial phonon DOSs of $Hf_{1-x}Si_xO_2$ with different Si-doping concentrations. (a) Total, (b) Hf, (c) Si, (d) O.

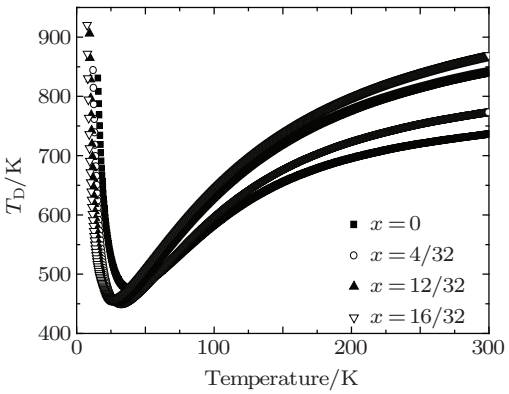

Fig. 8. Curves of Debye temperature (T_D) of $Hf_{1-x}Si_xO_2$ with different Si-doping concentrations and under temperatures less than 300 K.

4. Conclusion

Using an atomistic simulation technique, we studied the lattice structure and thermal properties of $Hf_{1-x}Si_xO_2$ with different Si-doping concentrations and at different temperatures. The main findings are as follows: 1) With the increase of the Si-doping concentration, the lattice constant of $Hf_{1-x}Si_xO_2$ reduces. With an increase in temperature or a decrease of pressure, the lattice constant increases. 2) Upon Si-doping, the distributions of the Hf/Si–O bond and the O–Hf/Si–O bond angle extend, indicating that the local lattice structure becomes somewhat disordered. 3) As the Si-doping concentration increases, both the bulk modulus and the shear modulus of $Hf_{1-x}Si_xO_2$ decrease; additionally they increase as temperature increases. 4) With the increase of the Si-doping concentration, the specific heat at a constant volume of $Hf_{1-x}Si_xO_2$ reduces. As temperature increases from 0 K to 400 K, the specific heat increases rapidly, and when the temperature is higher than 400 K, the specific heat saturates to the Dulong–Petit limit. 5) With the increase of the Si-doping concentration, the coefficient of thermal expansion of $Hf_{1-x}Si_xO_2$ reduces. The Grüneisen parameter of $Hf_{1-x}Si_xO_2$ is about 0.95 at temperatures less than 100 K, and decreases when the Si-doping concentration increases. 6) Hf atoms only show a phonon contribution in a low-frequency region, and almost no contribution in a high frequency region. Doped-Si atoms move the phonon spectra toward the left. 7) Compared with Si-doped HfO_2, pure HfO_2 has the largest Debye temperature when the temperature is less than 25 K, but it has the lowest Debye temperature when the temperature is higher

than 50 K.

Acknowledgment

This work was performed at the Gansu Province Supercomputer Center, China.

References

[1] Weir B E, Silverman P J, Alam M A, Baumann F, Monroe D, Ghetti A, Bude J D, Timp G L, Hamad A, Oberdick T M, Zhao N X, Ma Y, Brown M M, Hwang D, Sorsch T W and Madic J 1999 *Technical Digest-International Electron Devices Meeting* **99** 437

[2] Min C, Paul V V, Mike C and William G 1988 *IEEE Electron Dev. Lett.* **19** 291

[3] Ouyang C Y, Wang D Y, Shi S Q, Wang Z X, Li H, Huang X and Chen L Q 2006 *Chin. Phys. Lett.* **23** 61

[4] He G, Zhang L and Mater J 2007 *Sci. Technol.* **23** 433

[5] Kukli K, Niinisto J, Tamm A, Lu J, Ritala M, Leskelä M, Matti P, Niinistö L, Song F, Williams P and Heys P N 2007 *Micr. Eng.* **84** 2010

[6] Wang J, Li H P and Stevens R 1992 *J. Mater. Sci.* **27** 5397

[7] Balog M, Schieber M, Michiman M and Patai S 1977 *Thin Solid Films* **41** 247

[8] Ruh R and Corfield P W R 1970 *J. Am. Ceram. Soc.* **53** 126

[9] Foster A S, Lopez Gejo F, Shluger A L and Nieminen R M 2001 *Phys. Rev.* B **65** 174117

[10] Lakhlifi A, Leroux C, Satre P, Durand B, Roubin M and Nihoul G 1995 *J. Solid State Chem.* **119** 269

[11] Chen W, Sun Q Q, Ding S J, Zhang D W and Wang L K 2006 *Appl. Phys. Lett.* **89** 152904

[12] Evarestov R, Bandura A and Blokhin E 2009 *Acta Mater.* **57** 600

[13] Tang C and Ramprasad R 2008 *Appl. Phys. Lett.* **92** 182908

[14] Tang C, Tuttle B and Ramprasad R 2007 *Phys. Rev.* B **76** 073306

[15] Tang C and Ramprasad R 2008 *Appl. Phys. Lett.* **92** 182908

[16] Medvedeva N I, Zhukov V P, Khodos M Y and Cubanov V A 1990 *Phys. Stat. Sol.* **160** 517

[17] Carav M A and Casali R A 2005 *J. Phys.: Condens. Matter* **17** 5795

[18] Xu B, Liu Z T and Feng L P 2008 *J. Optoelectron. Laser* **19** 1645 (in Chineses)

[19] Zheng J X, Ceder G, Maxisch T, Chin W K and Choi W K 2007 *Phy. Rev.* B **75** 104112

[20] Tang F L, Yue R and Lu W J 2011 *Chin. Phys.* B **20** 026801

[21] Tang F L and Zhang X 2006 *Phys. Rev.* B **73** 144401

[22] Lu W J, Xie Y, Chen G B and Tang F L 2011 *Physica* B **406** 1289

[23] Gale J D and Rohl A L 2003 *Mol. Simulat.* **29** 291

[24] Shi S Q, Zhang H, Ke X Z, Ouyang C Y, Lei M S and Chen L Q 2009 *Phys. Lett.* A **373** 4096

[25] Shi S Q, Ke X Z, Ouyang C Y, Zhang H, Ding H C, Tang Y H, Zhou W W, Li P J, Lei M S and Tang W H 2009 *J. Power Sources* **194** 830

[26] Bourova E, Parker S C and Richet P 2000 *Phys. Rev.* B **62** 12052

[27] Tsuneyuki S, Tsukada M and Aoki H 1988 *Phys. Rev. Lett.* **61** 869

[28] Bongiorno A and Pasquarello A 2004 *Phys. Rev.* B **70** 195312

[29] Shannon R D 1976 *Acta Cryst.* A **32** 751

[30] Tang Q H 2009 *Comput. Mater. Sci.* **45** 429

[31] Zhu D M and Weng H F 1995 *J. Non-cryst. Solids.* **185** 262

[32] Zhou W, Shi Q, Woodfield B F and Navrotsky A 2011 *J. Chem. Thermodyn.* **43** 970

[33] Senyshyn A, Kraus H, Mikhailik V B and Yakovyna V 2004 *Phys. Rev.* B **70** 214306

[34] Xiang Y T, Jamnik A and Yang K W 2010 *Chin. Phys.* B **19** 110505

[35] Hou R L, Peng J X and Jing F Q 2009 *Acta Phys. Sin.* **58** 6413 (in Chinese)

[36] Yang T X, Cheng Q, Xu H B and Wang Y X 2010 *Acta Phys. Sin.* **59** 4919 (in Chinese)